Evolutionary rescue and reintroduction of resistant frogs allows recovery in the presence of a lethal fungal disease

Roland A. Knapp[a,b], **Mark Q. Wilber**[c,1], **Allison Q. Byrne**[d,e,1], **Maxwell B. Joseph**[f,g], **Thomas C. Smith**[a,b], **Andrew P. Rothstein**[d,e], **Robert L. Grasso**[h], **and Erica Bree Rosenblum**[d,e]

[a]Sierra Nevada Aquatic Research Laboratory, University of California, Mammoth Lakes, CA, 93546; [b]Earth Research Institute, University of California, Santa Barbara, CA, 93106-3060; [c]School of Natural Resources, University of Tennessee Institute of Agriculture, Knoxville, TN, 37996; [d]Department of Environmental Science, Policy, and Management, University of California - Berkeley, Berkeley, CA, 94720-3114; [e]Museum of Vertebrate Zoology, University of California - Berkeley, Berkeley, CA, 94720-3160; [f]Earth Lab, University of Colorado, Boulder, CO, 80303; [g]Planet, San Francisco, CA, 94107; [h]Resources Management and Science, Yosemite National Park, El Portal, CA, 95318

This manuscript was compiled on May 13, 2023

Escalating anthropogenic change is devastating global biodiversity. To avoid extinction, affected populations will often need to adapt to the altered environment. The process of rapid evolutionary change that increases the frequency of adaptive alleles and thereby restores positive population growth is termed "evolutionary rescue". In addition to allowing recovery of extant populations, individuals from rescued populations could also be used to reestablish extirpated populations. We evaluated this scenario in the once-common mountain yellow-legged (MYL) frog, which is threatened with extinction by the human-facilitated emergence of a lethal fungal pathogen (*Batrachochytrium dendrobatidis*; "Bd"). Although most MYL frog populations are extirpated following disease outbreaks, some persist and eventually begin to recover. We show that MYL frogs have undergone substantial evolutionary change following disease outbreaks, and that these changes are associated with increased resistance/tolerance to Bd infection in naturally recovering populations. Large-scale reintroduction of frogs from these populations resulted in the establishment of reproducing populations at most recipient sites despite ongoing disease. In addition, results from viability modeling suggest that established populations have a low probability of extinction over 50 years. Collectively, these results provide one of the first examples of how evolutionary rescue and the reintroduction of resistant/tolerant individuals can allow the landscape-scale recovery of disease-impacted species. This example has potentially broad implications for the many taxa worldwide that are threatened with extinction by anthropogenic stressors.

Human activities are intensifying threats to global biodiversity (1), with important implications for ecosystem resilience and human welfare (2). To persist, affected taxa will often need to adapt to their altered environment or face decline and extinction. "Evolutionary rescue" describes rapid evolutionary change that increases the frequency of adaptive alleles and thereby restores positive population growth (3). In addition to preventing extinction of declining populations, this process could also result in the seeding of nearby empty habitats and allow population reestablishment and recovery. Although this overall scenario is potentially of critical importance for the conservation of an ever-growing number of threatened taxa, descriptions of its operation in the wild are lacking.

One consequence of human alteration of the biosphere is an increase in emerging infectious diseases (4, 5). Such diseases pose a severe threat to wildlife populations (6), and have caused dramatic declines and extinctions in a wide range of taxa (7–10). Amid this global loss of biodiverity, some populations decimated by disease have subsequently recovered to varying extents (11–13). Although we know relatively little about the mechanisms underlying recovery (14, 15), host evolution is one possibility (3, 16). This process is known from a diversity of wildlife populations (17–20), and often results in increased host resistance and/or tolerance (see (21) for definitions). However, linking these evolutionary responses to population recoveries is difficult and few clear examples exist. In addition to promoting recovery of disease-impacted populations, the resistant/tolerant individuals in such populations could potentially be used to reestablish populations that were extirpated following disease emergence (14, 22). To date, the use of resistant/tolerant individuals for species recovery is rare (but see 23), and studies that evaluate its potential utility are critically needed.

The mountain yellow-legged (MYL) frog, composed of the sister species *Rana muscosa* and *Rana sierrae* (24), is emblematic of the unprecedented global declines of amphibians caused by the recently-emerged amphibian chytrid fungus (*Batrachochytrium dendrobatidis*, 9). Once the most common amphibian in the high elevation portion of California's Sierra

Significance Statement

Understanding how species persist despite accelerating global change is critical for the conservation of biodiversity. One possibility is rapid evolution that restores positive growth to declining populations ("evolutionary rescue"). Individuals from these rescued populations could also be used to reestablish exinct populations. We evaluated both possibilities in a once-common frog species driven to the brink of extinction by a disease that has devastated global amphibian biodiversity and for which few options exist to reverse disease impacts. We found that frogs have evolved increased resistance to infection, facilitating population recovery. In addition, introduction of frogs from these populations allowed reestablishment despite the ongoing presence of disease. Such reintroductions could play an important role in biodiversity conservation in our rapidly changing world.

[1]M.W. contributed equally to this work with A.B.

[2]To whom correspondence should be addressed. E-mail: roland.knapp@ucsb.edu

Nevada mountains (USA, 25), during the past century this frog has disappeared from more than 90% of its historical range (24). Due to the severity of its decline and the increasing probability of extinction, both species are now listed as "endangered" under the U.S. Endangered Species Act. In the Sierra Nevada, this decline was initiated by the introduction of non-native trout into the extensive historically-fishless region (26, 27) starting in the late 1800s. The arrival of *B. dendrobatidis* (Bd) in the 1960s and its subsequent spread (28) caused additional large-scale population extirpations (29, 30). These Bd-caused declines are fundamentally different from the fish-caused declines because removal of fish populations is feasible and results in the rapid recovery of frogs (31, 32). In contrast, Bd appears to persist in habitats even in the absence of amphibian hosts (33), and therefore represents a long-term alteration of invaded ecosystems that amphibians will need to overcome to reestablish populations.

Despite the catastrophic impact of Bd on MYL frogs, wherein most Bd-naive populations are extirpated following Bd arrival (29), some populations have persisted after epizootics (34) and are now recovering (13). Frogs in these recovering populations show reduced susceptibility to Bd infection, consistent with selection for more resistant/tolerant genotypes (13). Furthermore, exploratory efforts to reintroduce frogs collected from recovering populations to sites from which frogs were previously extirpated indicate that population establishment is possible despite ongoing Bd infection (23).

In the current study, we combine results from genomic analyses, a 15-year landscape-scale frog reintroduction effort, and a detailed population model to provide an unprecedented example of how evolution in response to disease allows the successful reestablishment of extirpated MYL frog populations. Specifically, we used exome capture methods to show that MYL frogs have undergone substantial evolutionary change associated with Bd exposure and that might provide a genetic basis for the increased resistance/tolerance to Bd infection observed in naturally recovering populations (13). We then use the reintroduction of resistant/tolerant frogs to 24 sites and results from long-term capture-mark-recapture (CMR) surveys to describe the dynamics and drivers of population establishment. These data are also used to parameterize a population model that extends our inferences of population establishment well beyond the temporal extent of the CMR data. Collectively, these results provide one of the first examples of how evolutionary rescue and the reintroduction of resistant/tolerant animals can allow the large-scale recovery of disease-impacted species.

Results

Frog evolution in response to Bd. To determine whether MYL frog populations show an evolutionary response to Bd, we compared frog genomes between populations with contrasting histories of Bd exposure. Specifically, we compared frog genomes sampled in four populations that have not yet experienced a Bd-caused epizootic ("naive") (35) versus in five populations that experienced a Bd epizootic during the past several decades and have since recovered to varying degrees ("recovering"; Figure 1) (13, 29). These recovering populations exist in an enzootic state (34), characterized by high Bd prevalence and, in adults, moderate Bd infection intensities ("load") that are typically well below the level expected to cause mortality (29).

We conducted a principal component analysis (PCA) of the genomic data to describe the relationships between sampled populations, and then used two complementary approaches to identify regions of the genome under selection. First, we used a multivariate linear mixed model to evaluate associations between population type (i.e., naive versus recovering) and individual variants, including single nucleotide polymorphisms (SNPs) and insertions/deletions (INDELS). Second, we used a splined window analysis to identify larger genomic regions showing differences between population types in F_{ST} and nucleotide diversity ($\pi_{diff} = \pi_{naive}$ - $\pi_{recovering}$).

Individual frogs clustered into 3 separate groups in principal component space (Figure S1A), and clusters reflected the strong signature of isolation by distance that is characteristic of MYL frogs (36, 37). Importantly, each cluster contained at least one population from both the naive and recovering groups, allowing us to distinguish allelic associations of individuals sampled in the 2 population types versus allelic associations resulting from population structure and genetic drift.

Results from the individual variant and splined window analyses show that recovering populations have signatures of strong selection on multiple regions of the genome. The analysis of individual variants identified 11 "outlier" SNPs (i.e., showing significantly different allele frequencies between naive versus recovering populations) from 7 distinct genes across 4 contigs (Figure S1B,C). One of the 7 identified genes did not have an associated annotation. Frequency differences between the naive and recovering populations ranged from 41% to 86%. Most of these SNPs showed frequency differences in only a subset of the sampled populations (Figure 1 A, B), but the SNP in the RIN3 gene showed consistent differences in frequencies across all populations (Figure 1 C). This is suggestive of strong - and parallel - selection at this locus associated with exposure of frogs to Bd across multiple populations.

The splined window analysis identified 33 outlier regions for π_{diff} and 58 outlier regions for F_{ST} (Figure 2 A, B). Of these, 9 regions were outliers for both metrics and 2 of these shared regions also contained outlier SNPs. A total of 33 annotated genes were found in the 9 shared regions (SI). The largest π_{diff}, indicative of directional selection, occurred in a 163kb region on Contig19, 12.9Mb upstream of the RIN3 outlier SNP (Figure 2 C). This region contains approximately 500 SNPs and one annotated gene called "interferon-induced very large GTPase 1-like" (GVINP1). Additionally, a shared outlier region on Contig1 contained two complement factor genes (C6 and C7). Interestingly, this region had a low π_{diff} value, consistent with balancing selection. Finally, one shared outlier region on Contig8 contained one outlier SNP (TCF19) and was within 360kb of another outlier SNP (VARS) (Figure 2 D, Figure S2). This region (854kb from the beginning of the outlier window to the VARS SNP) contained a total of 8 annotated genes. In *Xenopus*, five of these genes occur in the extended major histocompatibility complex (MHC) Class I region (FLOT1, TUBB, MDC1, CCHCR1, TCF19) and three occur in the extended MHC Class III region (HSP70, LSM2, VARS) (38). Therefore, this region under selection is part of the extended MHC Class I and III complex and shows synteny with other amphibian genomes.

Frog population recovery. To determine whether *R. sierrae* from recovering populations could be used to reestablish

extirpated populations, we conducted 24 reintroductions in Yosemite National Park (2006–2020). Each of the reintroductions involved collection of adult frogs from 1 of 3 recovering, Bd-positive "donor" populations (Figure S3) and translocating them to 1 of 12 nearby recipient sites (39). The donor populations included 2 of the 5 recovering populations in the frog evolution study described above (Figure 1 A: population 1 and 4). Following translocation, adult survival and recruitment of new adults were estimated from CMR surveys and counts of tadpoles and juveniles were obtained from visual encounter surveys (VES).

Estimates of frog survival during the 1 year following translocation indicate that survival was highly variable between recipient sites, but relatively constant within recipient sites (for the subset of sites that received multiple translocations; Figure 3). As such, the average survival of frogs in the first translocation to a site was an important predictor of survival of frogs in subsequent translocations to that site (Figure S4). This suggests an important effect of site characteristics and/or (site * frog) interactions on frog survival. In addition, 1-year survival was higher for frogs translocated later in the study period than earlier (Table S1), which we suggest resulted primarily from our improved ability over time to choose recipient sites with higher habitat quality for *R. sierrae*. Finally, Bd loads were fairly consistent before versus after translocation and loads were nearly always well below the level indicative of severe chytridiomycosis and associated frog mortality (Figure S5, see SI text for additional details) (23, 29).

Of the 12 translocated populations, 9 (0.75) showed evidence of successful reproduction in subsequent years, as indicated by the presence of tadpoles and/or juveniles. For these 9 populations, one or both life stages were detected in nearly all survey-years following translocation (proportion of survey-years: median = 0.9, range = 0.29–1). These same populations were also those in which recruitment of new adults (i.e., progeny of translocated individuals) was detected. As with early life stages, recruits were detected in the majority of post-translocation survey-years (proportion of survey-years: median = 0.79, range = 0.12–1). In summary, survey results suggest that translocations resulted in the establishment of reproducing MYL frog populations at most recipient sites despite the ongoing presence of Bd.

To determine whether Bd load had a negative effect on adult survival, as would be expected if frogs were highly susceptible to Bd infection, we developed linear and multilevel models. The best model of 1-year frog survival identified several important predictors, but Bd load at the time of translocation was not among them (bd_load; Figure S6). Important predictors included winter severity in the year following translocation (snow_t1), site elevation (elevation), and donor population (donor_72996; Figure 4). Males had somewhat higher survival than females, but this effect was only marginally important (sex_male; Figure 4, Figure S6). Collectively, these results are consistent with frogs in recovering populations having evolved sufficient resistance/tolerance to minimize the adverse effects of Bd infection. In addition, the moderate Bd loads that characterized frogs following translocation (Figure S5) and relatively high survival of frogs in numerous translocated cohorts (Figure 3) suggests that frogs translocated from recovering populations can maintain the benefits of resistance/tolerance in non-natal habitats. Finally, in 3 locations where longer CMR time series allowed us to assess the survival of new adults recruited to the population, naturally recruited adults had equivalent or higher survival probabilities than the originally translocated adults (Figure S7). Therefore, frog resistance/tolerance in non-natal habitats is maintained across generations.

Long-term population viability. Results from frog translocations indicated that adult survival was often relatively high and that most populations showed evidence of successful reproduction and recruitment (described above). Although suggestive of population establishment, a decade or more of surveys may be necessary to confirm that populations are in fact self-sustaining (23). To extend our inferences of population establishment beyond those possible from the 2-16 years of site-specific CMR data, we developed a population viability model. Specifically, to test whether the observed yearly adult survival probabilities in translocated populations were sufficient to promote long-term viability, we built a stage-structured matrix model that captured known frog demography and included demographic and environmental stochasticity. We parameterized the model using CMR data from translocated populations and known life history values in this system (Table S2).

Given observed yearly adult survival probabilities (from analysis of CMR data) and a baseline yearly recruitment probability ω of 0.3 (i.e., the probability that, following survival, juveniles successfully recruit to the adult class), our stage-structured model predicted that six of twelve translocated populations should experience a long-run growth rate λ greater than 1 in the presence of Bd (Figure 5 A; median predicted λ ranges from 1.15-1.36 for these six populations). These six populations all had observed yearly adult survival greater than 0.5. When we reduced the probability of successful recruitment ω to 0.1 (a highly conservative estimate), long-run growth rate of five of these six populations was still greater than 1 (Figure 5 A).

Even when incorporating demographic stochasticity and environmental stochasticity in the probability of juvenile recruitment to the adult class ω (the transition that we expect to be the most subject to environmental variability in the presence of Bd), populations with high adult survival are likely to persist over a 50 year time horizon. Our model predicted that, following a single introduction of 40 adult individuals into a population and using the baseline value for ω of 0.3, the six populations with the highest adult survival probabilities had 50-year extinction probabilities of 0 to 0.32; Figure 5 B). This indicates strong potential for long-term persistence in the presence of Bd and environmental variability in recruitment (Figure 5 B). When we decreased ω from 0.3 to a conservative estimate of 0.15, 50-year extinction probability remained less than 0.5 for three populations and was 0.79 to 0.94 for three additional populations (Figure 5 B). In contrast, for the six populations where yearly adult survival probability $\sigma_{A_R} < 0.5$, extinction probability over 50 years was always predicted to be 1. To test the validity of our model predictions, we demonstrated that our stochastic model could describe the general recovery trajectory of our translocated population with the longest survey history (Figure 5 C; population 70550, surveyed for 16 years).

In summary, our model demonstrates that given observed yearly adult survival probabilities of translocated frogs, 50%

of our translocated populations have a high probability of population growth and long-term viability in the presence of Bd. This is likely a conservative estimate because there is evidence that naturally-recruited adults have higher survival probability than translocated adults (Figure S7), but we considered these probabilities to be equal in all but three of our populations where we had sufficient data to distinguish these different probabilities. In addition, 5 of the 7 populations translocated after 2013 were predicted to have long-term viability, compared to only 1 of 5 populations translocated prior to 2013 (Table S1). Thus, there is some trend suggesting that our ability to select high quality habitats that promote long-term viability of translocated populations improved over time.

Discussion

Disease-induced population declines are decimating global biodiversity (6), but strategies to recover affected species are generally lacking. Here, we used populations of resistant/tolerant individuals to reestablish extirpated populations, despite ongoing disease. Although previously proposed (22), this strategy has rarely been successfully implemented (see (23) for a small-scale example). In particular, although numerous studies have documented signatures of selection in hosts following disease-induced declines (e.g., 18, 19), we are unaware of any that used individuals bearing the resulting adaptive alleles to reestablish extirpated populations. The results of our study provide evidence that (i) MYL frogs have experienced strong selection following exposure to a recently-emerged lethal fungal disease and that some of the genomic regions under selection are associated with genes related to disease resistance/tolerance, and (ii) reintroduction of individuals from these resistant/tolerant populations allows the successful reestablishment of viable frog populations despite ongoing Bd infection.

Previous field studies in MYL frogs show that frog-Bd dynamics and frog survival in the presence of Bd are fundamentally different between naive and recovering populations. Following the arrival and establishment of Bd in previously-naive populations, adult frogs develop high Bd loads that lead to mass die-offs (29). In contrast, in recovering populations adult frogs typically have low-to-moderate and relatively constant Bd loads and mass die-offs are not observed (34, 40, see also Figure S5 - before translocation). The differences in Bd load of frogs from naive and recovering populations are also observed in controlled laboratory studies (13, Figure 4). The observed reduced susceptibility of frogs from recovering populations could in theory be due to several factors including natural selection for more resistant/tolerant genotypes and/or acquired immunity, but until now evidence to evaluate the role of evolution was lacking.

Results from our genomic analyses strongly suggest that natural selection for adaptive alleles and resulting increased resistance/tolerance is at least partially responsible for the reduced susceptibility of frogs in recovering populations. We identified specific alleles and genomic regions showing signatures of selection between adjacent Bd-naive and recovering MYL frog populations, consistent with strong selection following Bd exposure. Importantly, some regions under selection are associated with cellular and immunological mechanisms known to contribute to disease resistance, including in amphibians (41). For example, the MHC plays an important role in immunity. In our study, we identified a region that shows evidence of selection in recovering populations and contains eight genes associated with either the MHC Class I or Class III regions. These results corroborate numerous previous studies linking MHC genes to amphibian resistance/tolerance against Bd (e.g., 42, 43). Similarly, the region with the strongest indication of directional selection (as measured by π_{diff}) contains the gene GVINP1. Several previous studies have found this gene to be differentially expressed during Bd infection (e.g., 44, 45) and in populations differing in Bd susceptibility (44). This gene is also strongly linked to disease in salmon, explaining a notable 20% of the resistance phenotype (46, 47). We also identified a region, characterized by high F_{ST} and low π_{diff}, that contained the complement genes C6 and C7. This could indicate that balancing selection is acting in this region of the genome to favor a diverse set of alleles, as is known for C6 in humans (48). Finally, the RIN3 gene showed a consistent pattern of allele frequency differences across all nine of the frog populations sampled in this study, indicating consistent selection in populations distributed across a wide geographic area. This gene is associated with inflammation response and in *Xenopus* is highly expressed in wound stumps following amputation of tadpole tails (49). In the SI, we provide additional details on these and other genes identified in our study as under selection.

Reintroduction of resistant/tolerant MYL frogs was remarkably successful in reestablishing viable populations in the presence of Bd. Of the 12 translocated populations, approximately 80% showed evidence of both successful reproduction and recruitment of new adults. Bd loads measured before and after translocation were similar and generally remained well below the level at which frog mortality occurs. Annual survival for 12 of the 24 translocated cohorts exceeded 50%, and > 70% of translocated cohorts had survival above this 50% level when the earliest translocations are excluded (i.e., translocations conducted when methods were still being refined). The fact that the relatively low Bd loads and correspondingly high frog survival in the presence of Bd was maintained between the natal/donor sites and the recipient sites indicates that these characteristics of naturally-recovering populations were not solely an effect of the natal/donor site or site * frog interactions, but instead were due at least in part to resistance/tolerance inherent in the frogs. In addition, the relatively high survival of translocated frogs was maintained in their progeny, as expected if resistance/tolerance has a genetic basis. Results from the population viability model were also encouraging. In particular, translocated populations with > 50% survival in the first year post-translocation were predicted to have a low probability of extinction over 50 years (probability of extinction = 0 - 0.32). In light of the generally low success rate of amphibian reintroduction efforts (50), our success in reestablishing MYL frog populations via translocation of resistant/tolerant individuals is striking, and even more so given that this success occurred despite ongoing infection of frogs with Bd.

Despite the resistance/tolerance of adult MYL frogs in recovering populations, individual and population-level impacts of Bd are still evident. In an earlier study of 2 of our 12 translocated populations, Bd infection and load had detectable effects on the survival of adults and may have influenced population establishment (sites referred to as “Alpine” and “Subalpine” in

(23) are identified as "70550" and "70505" in the current study). Applying similar analyses to all 12 of our translocated populations would likely provide a broader perspective of the ongoing effect of Bd. In addition to these important but relatively subtle effects on adults, MYL frogs immediately following metamorphosis ("metamorphs") are highly susceptible to Bd infection (51) and experience high mortality. This high susceptibility of metamorphs is documented for numerous species of anurans, and may result from the poorly developed immune system characteristic of this early life stage (52). In naturally recovering and translocated MYL frog populations, we suggest that the high mortality of metamorphs is an important limitation on subsequent recruitment of new adults. Therefore, although adult MYL frogs appear relatively resistant/tolerant, Bd infection continues to have important limiting effects on recovering populations (see also 53).

The recent emergence of Bd worldwide has contributed to the decline of hundreds of amphibian species, some of which are now extinct in the wild (9). This unprecedented impact on global amphibian biodiversity is compounded by the lack of any effective and broadly applicable strategies to reverse these impacts (54, 55). Importantly, in addition to the natural recovery documented for MYL frogs (13), other species are also showing evidence of post-epizootic recovery in the presence of Bd (12, 56) and suggest the possibility of also using animals from these recovering populations to reestablish extirpated populations. As with MYL frogs, the feasibility and long-term success of such efforts will depend on the availability of robust donor populations containing individuals that have acquired via evolution the adaptive alleles necessary to allow frog survival and population growth in the presence of Bd. Despite the hopeful example of successful reestablishment of MYL frogs via evolutionary rescue and reintroductions, the challenge of recovering hundreds of Bd-impacted amphibian species worldwide is a daunting prospect. Although we now have a proven strategy to reestablish extirpated MYL frog populations, recovery across their large historical range will require substantial resources over many decades. The results of this study provide a hopeful starting point for that endeavor, and other future efforts worldwide.

Evolutionary rescue may be increasingly critical for the survival of wildlife populations in a rapidly changing world. The importance of evolutionary rescue is known for a wide variety of taxa (e.g., 3, 57, 58), including in the specific context of disease-impacted systems (16). However, obtaining evidence in wild animal populations for all the causal links in this process (i.e., selection for adaptive alleles → increase in host fitness in the presence of the stressor → positive population growth and recovery) is difficult in most systems. Nonetheless, we provide a compelling example from the wild not only that evolutionary rescue can produce individuals that harbor adaptive alleles and allow population recovery, but importantly that these individuals can be used in translocations to reestablish extirpated populations. We expect that such "assisted evolutionary rescue" will be an essential tool in wildlife conservation in an era of accelerating global change.

Materials and Methods

Frog evolution in response to Bd

Sampling and Sequencing. We collected DNA samples via buccal swabbing (59) from 53 *Rana muscosa*/*Rana sierrae* individuals: 24 from four Bd-naive populations, and 29 from five recovering populations. These populations were located in the southern Sierra Nevada, from northern Yosemite National Park to northern Sequoia National Park (Figure 1). Samples were collected from 5-6 frogs per population. To minimize potential confounding effects caused by variation in frog genotypes across latitude (e.g., 36), we selected sampling sites such that both population types were represented across similar latitudinal ranges. DNA was extracted following Qiagen DNEasy manufacturer's protocols. We sequenced the samples using an exome capture assay as described in Byrne et al. (in review). Briefly, genomic libraries were prepared and captured using a custom Nimblegen capture pool. Capture baits were designed based on the coding regions of the *R. muscosa* transcriptome (GenBank accession GKCT00000000). Captured libraries were then pooled and sequenced on a NovaSeq 6000 150PE Flow Cell S1 at the Vincent J. Coates Genomics Sequencing Lab at UC Berkeley.

Data Pre-processing and Cleaning. Raw reads were filtered for adapters and contaminants using fastp (60) and aligned to the *Rana muscosa* genome (NCBI SRA: SRS6533475, reference = 61) with repetitive elements masked using bwa ("mem" mode) (62). Exact PCR Duplicates were marked using Picard. Variants were then called following GATK best practices (v.4.2.0.0, (63)). Briefly, raw variants were called for each sample using HaplotypeCaller and combined using CombineGVCFs. Next, genotypes were jointly called using GenotypeGVCFs. Variants were then hard filtered using gatk VariantFiltration using the following parameters to remove low-quality sites: QD $<$ 2.0, FS $>$ 40.0, SOR $>$ 3.0, MQ $<$ 50.0, MQRankSum $>$ 3.0, MQRankSum $<$ -3.0, ReadPosRankSum $>$ 3.0, ReadPosRankSum $<$ -3.0. This initial filter resulted in 1,595,206 variant sites across 53 individuals.

We then further filtered our dataset at the individual and variant level. First, we trimmed our variants to only include those with minor allele frequency $>$ 0.03, a maximum depth of 250 and minimum depth of 5, a minimum genotype quality of 20, and a maximum missing proportion of 0.5. This filter resulted in 427,038 sites, of which 353,172 were single nucleotide polymorphisms (SNPs) and 73,866 were insertions or deletions (INDELS). Finally, we trimmed samples with an average depth across filtered sites $<$ 7x. Our final dataset included 50 samples (23 from naive and 27 from recovering populations) with an average depth of 16.7x (range = 7.4x – 26.1x).

Data Analysis. To visualize the genomic relationship of our populations we conducted a principal components analysis (PCA) using the glPCA function in the adegenet R package (64). To detect regions of the genome under selection between naive and recovering populations, we used two approaches: (1) a multivariate linear mixed model to evaluate individual variants (SNPs and INDELs), and (2) a splined window analysis to evaluate larger genomic regions. For the variant analysis, we first used a stringent data filter to include only variants with $<$ 5% missing data (missing for no more than 2 individuals), and then calculated the likelihood ratio statistic for the resulting set of 148,307 high quality variants across 127 contigs using GEMMA. GEMMA calculates and incorporates a relatedness matrix for input samples, allowing us to account for relatedness and population structure when calculating likelihood ratio statistics. We identified variants showing different allele frequencies between naive versus recovering populations ("outliers") using a Bonferroni-corrected significance level of 0.01. We visualized the results using a Manhattan plot and qqplot. We developed a more liberal set of outlier variants using a Bonferroni- corrected significance level of 0.05 and used this set solely for the gene ontology (GO) analysis (see below and SI).

For each outlier variant, we determined whether the variant was synonymous (protein sequence the same for each variant) or non-synonymous (protein sequence differs between variants), and where in the gene it was located. To do this, we first extracted the reference genome sequence surrounding the variant using the bedtools "getfasta" function (65). Next, we re-annotated each sequence using blast to get the predicted gene location based on the closest annotated reference (66). We then translated each variant

to amino acids and aligned this translation to that of the gene annotation to ensure proper frame of reference using Geneious (67). After ensuring proper translation, we characterized variants as within or outside the coding sequence of the gene and as either synonymous or non-synonymous.

In the splined window analysis, we identified outlier regions using F_{ST} and differences in nucleotide diversity (π_{diff}) between naive and recovering populations. First, we calculated per-site F_{ST} between the naive and recovering individuals for all bi-allelic SNPs in the 30 largest contigs (98% of all SNPs) using VCFtools (68). Next, we calculated per-site nucleotide diversity π separately for individuals from the naive and recovering populations using VCFtools, then calculated π_{diff} for each population ($\pi_{diff} = \pi_{naive} - \pi_{recovering}$). We concatenated the values for F_{ST} and π_{diff} in order of size-sorted chromosome number and adjusted the SNP position based on the relative position in the genome. We then used the WINGEN R package (69) to conduct a splined discrete window analysis for F_{ST} and π_{diff}. This method calculates where non-overlapping window boundaries should occur by identifying inflection points in the fitted spline, therefore balancing false positive and false negative results that occur using other window-based methods (70) . This method also calculates a W-statistic allowing for outlier identification. We identified outliers as those with a W-statistic greater than 4 standard deviations above the mean for F_{ST} or above/below the mean for π_{diff}. Outlier regions were then identified as those that were outliers in both analyses, meaning that they showed 1) high differentiation between naive and recovering populations, and 2) differential patterns of nucleotide diversity in the same region. Finally, we extracted gene transcripts mapped within each region and retrieved annotation for that region using blast.

Using the liberal set of variant outliers, we performed a statistical overrepresentation test (Fisher's exact test) using Blast2GO (71). First, we retrieved the Blast hits and mapped GO terms for each gene in our targeted transcriptome. Next, we compared the 29 unique outlier genes from the liberal set of outlier variants to the complete set of genes in our target transcriptome to determine if any GO biological functions, molecular functions, or cellular processes were overrepresented. We then repeated this process for the set of 33 genes located in the overlapping F_{ST} and π_{diff} splined windows. Code used for genomic analyses and to figures is available from the following GitHub repository: https://github.com/allie128/mylf-selection.

Frog population recovery

Field methods. For the 24 translocations we conducted, we identified donor populations from which adult frogs ($\geq$ 40 mm snout-vent length) could be collected using several years of visual encounter surveys (VES) and skin swab collections (13), as well as landscape genetic information (37). The populations that we selected contained several hundred *R. sierrae* adults and hundreds or thousands of tadpoles. These relatively high abundances were the result of recent increases following previous Bd-caused declines (13). As is typical for recovering MYL frog populations, Bd prevalence in the donor populations was high (0.69–0.96) and Bd load (median $\log_{10}$(load) = 3.06–3.78 ITS copies) was two or more orders of magnitude below the level at which frog mortality is expected ($\log_{10}$(load) $\approx$ 5.78 copies)(23, 29). Recipient sites to which frogs were translocated were chosen based on previous *R. sierrae* presence (determined from VES and/or museum records) or characteristics that suggested high quality habitat for this species (72).

We conducted 1–4 translocations per site (Figure S3) and each translocated cohort included 18 to 99 frogs (median = 30). During each translocation, adult frogs were collected from the donor population and measured, weighed, swabbed, and PIT tagged. Frogs were transported to the recipient site either on foot or via helicopter. Following release, translocated populations were visited approximately once per month during the summer active season (median number of visits per summer = 2; range = 1–10) and assessed using diurnal CMR surveys and VES. CMR surveys allowed quantification of adult survival, adult population size, and recruitment of new adults, and VES provided estimates of tadpole and juvenile abundance. During 2006-2012, CMR surveys were conducted on a single day (primary period) per site visit, during which all habitats were searched repeatedly for adult frogs. Frogs were captured using handheld nets, identified via their PIT tag (or tagged if they were untagged), measured, weighed, swabbed, and released at the capture location. During 2013-2022, we generally used a robust design in which all habitats were searched during several consecutive days (median number of secondary periods per primary period = 3; range = 3–7), and frogs were processed as described above. However, when the number of frogs detected on the first survey day was zero or near zero, we typically conducted only a single-day CMR survey. When using a robust design, within a primary period, frogs that were captured during more than one secondary period were measured, weighed, and swabbed during the first capture, and during subsequent captures were only identified and released. Frog skin swabs were analyzed using standard Bd DNA extraction and qPCR methods. For details of survey and swab analysis methods, see (23).

During each site visit, we conducted VES either immediately before CMR surveys or during the first day of CMR surveys. VES was conducted by walking the entire water body perimeter, first 100 m of each inlet and outlet stream, and any fringing ponds and wetlands, and counting all *R. sierrae* tadpoles and juveniles. These *R. sierrae* life stages have high detectablility, and counts are highly repeatable and provide estimates of relative abundance (27).

Estimation of frog survival and abundance. We estimated survival of translocated frogs, recruitment of new frogs into the adult population, and adult population size using a Bayesian open-population Jolly-Seber mark-recapture model with known additions to the population (i.e., translocated cohorts), as implemented by the mrmr package (73) and using R Statistical Software (v4.4.4, 74). The model tracks the states of M individuals that comprise a superpopulation made up of real and pseudo-individuals (see 23, for details). The possible states of individuals include "not recruited", "alive", and "dead". The possible observations of individuals include "detected" and "not detected". We assume that individuals that are in the "not recruited" or "dead" states are never detected (i.e., there are no mistakes in the individual PIT tag records). For all models, we used mrmr defaults for priors, number of chains (4), and warmup and post-warmup iterations (2000 for each). We evaluated convergence of the Markov chain Monte Carlo (MCMC) algorithm using trace plots and Gelman-Rubin statistics (Rhat). Code used to create CMR datasets and fit models for each translocated population is available from the following GitHub repository: https://github.com/SNARL1/cmr-analysis.

Predictors of post-translocation frog survival. To identify important predictors of frog survival following translocation, we developed linear and multilevel models in a Bayesian framework. We performed all analyses with the rstanarm package (75) and R Statistical Software (v4.4.4, 74), and used default, weakly informative priors. Starting models included all relevant population-level effects and, when data contained possible hierarchical structure, we included group-level effects in the full model. Within each analysis, we evaluated model fit using visualizations of leave-one-out ("LOO") probability integral transformations (76, 77), and compared fits of models with and without group-level effects, and with differing group-level effects using LOO cross-validation (78). Both approaches utilized the loo package (79).

We conducted two analyses. In the first, we addressed the more general question of whether survival of frogs in the first translocation to a site predicted the survival of frogs in subsequent translocations. Group-level effects included site_id or translocation_id. The second analysis focused specifically on identifying predictors of post-translocation frog survival using a wide range of variables describing characteristics of frogs, sites, and translocations (predictor variables: Bd load (bd_load), winter severity in the year following translocation (snow_t1), site elevation (elevation), donor population (donor_72996), sex (sex_male), frog size (length), winter severity in the year of translocation (snow_t), day of year on which a translocation was conducted (day), and translocation order (order_first)). In both analyses we used 1-year survival as a single metric of survival that was available for all translocated populations regardless of how many years of post-translocation data were available (range = 3--16). Group-level effects included site_id, translocation_id, or translocation_id nested within site_id. In both analyses, the response variable, probability of 1-year frog survival, was rounded to

$$\begin{bmatrix} L_1 \\ L_2 \\ L_3 \\ J_1 \\ J_2 \\ A_R \\ A_T \end{bmatrix} (t+1) = \begin{bmatrix} 0 & 0 & 0 & 0 & 0 & \sigma_{A_R} p_F F & \sigma_{A_T} p_F F \\ \sigma_{L1} p_{L1} & 0 & 0 & 0 & 0 & 0 & 0 \\ 0 & \sigma_{L2} p_{L2} & 0 & 0 & 0 & 0 & 0 \\ \sigma_{L1}(1-p_{L1}) & \sigma_{L2}(1-p_{L2}) & \sigma_{L3} & 0 & 0 & 0 & 0 \\ 0 & 0 & 0 & \sigma_{J1} p_{J1} & 0 & 0 & 0 \\ 0 & 0 & 0 & \sigma_{J1}(1-p_{J1})\omega & \sigma_{J2}\omega & \sigma_{A_R} & 0 \\ 0 & 0 & 0 & 0 & 0 & 0 & \sigma_{A_T} \end{bmatrix} \begin{bmatrix} L_1 \\ L_2 \\ L_3 \\ J_1 \\ J_2 \\ A_R \\ A_T \end{bmatrix} (t) \qquad [1]$$

integer values to produce a binomial outcome, and all models used a bernoulli family. For all models, we used default priors, four chains, and 5000 iterations each for warmup and post-warmup. We checked convergence of the MCMC algorithm using trace plots and Rhat. Code to create the datasets and fit models is available from the following GitHub repository: https://github.com/SNARL1/translocation.

Changes in Bd load following translocation. We analyzed skin swabs using standard Bd DNA extraction and qPCR methods (80, see SI for details). To assess the magnitude of changes in Bd load on frogs following translocation, we compared Bd loads measured before versus after translocation. Before-translocation loads were quantified using skin swabs collected from all to-be-translocated frogs at the donor site on the day before or the day of the translocation. After-translocation Bd loads were based on all swabs collected from translocated frogs at the recipient site in the year of and the year following translocation. Individual frogs and their associated Bd loads were included in the dataset only if frogs were captured at the recipient site at least once during the year 0-1 period. We used an analysis workflow similar to that described above. Briefly, the response variable was before-translocation load and the predictor variable was after-translocation load. We compared models with and without group-level effects, and group-level effects included pit_tag_id, pit_tag_id nested within site_id, or pit_tag_id nested within translocation_id. All models used a negative binomial family. Priors, chains, iterations, and checks were as described above. Code to create the dataset and fit models is available from the following GitHub repository: https://github.com/SNARL1/translocation.

Population viability modeling

Model description. To determine the implications of observed 1-year adult survival on the long-term viability of populations established via translocation, we developed a population model for MYL frogs. Our central question was: How does the magnitude and variation in observed adult survival probability across translocated populations affect the long-term persistence probability of populations? We developed a model that tracked seven state variables of a frog population: density of translocated adults (A_T), density of adults naturally recruited into the population (A_R), density of first-year tadpoles (L_1), density of second-year tadpoles (L_2), density of third-year tadpoles (L_3), density of first-year juveniles (J_1), and density of second-year juveniles (J_2). We divided adults into two classes A_T and A_R because there is evidence that the survival probability of translocated adults and naturally recruited adults differs (Figure S7).

We modeled the dynamics of these seven state variables using a discrete-time, stage-structured model where a time step is one year. The dynamics are given by

The parameters in this model are yearly survival probability $\sigma_{\cdot}$ (the subscript "$\cdot$" indicates a particular state variable), probability that a female frog reproduces in a given year p_F, number of eggs produced by a female frog in a year that successfully hatch F, probability of a first-year tadpole remaining as a tadpole p_{L1}, probability of a second-year tadpole remaining as a tadpole p_{L2}, and probability of a first-year juvenile remaining as a juvenile p_{J1}, and the probability of a juvenile successfully recruiting to an adult ω.

In this model we ignore density-dependent recruitment because we were interested in the growth of the population from an initial reintroduction and whether this growth was sufficient to prevent extinction over 50 years following the introduction. We also did not directly consider the dynamics of Bd in this model. We made this decision because (i) translocated populations are infected with Bd at high prevalence (23), and (ii) host density does not seem to play a significant role in multi-year Bd infection dynamics in this system (81). Thus, ignoring Bd infection dynamics and instead assuming all host vital rates are in the presence of high Bd prevalence significantly simplifies the model without much loss of realism.

Model analysis. After parameterizing our model with CMR-estimated adult frog survival probabilities and other known vital rates (Table S2), we performed four analyses (described in detail in the SI). First, we compute the long-run growth rate λ for each of our 12 translocated populations to determine if the populations were deterministically predicted to grow or decline in the long-run. Second, we compute the elasticity of λ to model parameters, to quantify how much changes in adult survival, for example, affected the long-run growth rate. Third, we included demographic and environmental stochasticity into our model and simulated the 50-year viability (i.e., 1 - extinction probability) of populations given an introduction of 40 adult individuals into an unoccupied habitat. Finally, we fit our model to our longest translocation trajectory to confirm that our model could reasonably reproduce the observed recovery trajectories of MYL frogs following reintroductions.

ACKNOWLEDGMENTS. We thank the following for important contributions to this study: E. Hegeman and A. Lindauer–project and data management, field and laboratory work; A. Barbella and K. Rose–laboratory work; C. Kamoroff and numerous summer technicians–field work; staff at Sequoia-Kings Canyon and Yosemite National Parks, Inyo and Sierra National Forests, California Department of Fish and Wildlife, U.S. Fish and Wildlife Service, University of California-Santa Barbara Institutional Animal Care and Use Committee, and Sierra Nevada Aquatic Research Laboratory–research permits, logistical support, and/or field assistance. This project was supported by grants from the National Park Service (to R.A.K.), Yosemite Conservancy (to R.A.K.); and National Science Foundation Grants EF-0723563 (to C. Briggs), DEB-1557190 (to C. Briggs), DEB-2133401 (to M.Q.W), and DBI-2120084 (to C. Richards-Zawacki).

1. G Ceballos, et al., Accelerated modern human-induced species losses: Entering the sixth mass extinction. *Sci. Adv.* **1** (2015).
2. S Naeem, DE Bunker, A Hector, M Loreau, C Perrings, *Biodiversity, ecosystem functioning, and human wellbeing: an ecological and economic perspective*. (Oxford University Press), (2009).
3. SM Carlson, CJ Cunningham, PA Westley, Evolutionary rescue in a changing world. *Trends Ecol. & Evol.* **29**, 521–530 (2014).
4. KE Jones, et al., Global trends in emerging infectious diseases. *Nature* **451**, 990–993 (2008).
5. MC Fisher, et al., Emerging fungal threats to animal, plant and ecosystem health. *Nature* **484**, 186–94 (2012).
6. P Daszak, AA Cunningham, AD Hyatt, Emerging infectious diseases of wildlife – threats to biodiversity and human health. *Science* **287**, 443–449 (2000).
7. I Hewson, et al., Densovirus associated with sea-star wasting disease and mass mortality. *Proc. Natl. Acad. Sci. USA* **111**, 17278–17283 (2014).
8. MD Samuel, BL Woodworth, CT Atkinson, PJ Hart, DA LaPointe, Avian malaria in Hawaiian forest birds: infection and population impacts across species and elevations. *Ecosphere* **6**, art104 (2015).
9. BC Scheele, et al., Amphibian fungal panzootic causes catastrophic and ongoing loss of biodiversity. *Science* **363**, 1459–1463 (2019).
10. CX Cunningham, et al., Quantifying 25 years of disease-caused declines in Tasmanian devil populations: host density drives spatial pathogen spread. *Ecol. Lett.* **24**, 958–969 (2021).
11. DA Newell, RL Goldingay, LO Brooks, Population recovery following decline in an endangered stream-breeding frog (*Mixophyes fleayi*) from subtropical Australia. *PLoS ONE* **8**, e58559 (2013).
12. J Voyles, et al., Shifts in disease dynamics in a tropical amphibian assemblage are not due to pathogen attenuation. *Science* **359**, 1517–1519 (2018).

13. RA Knapp, et al., Large-scale recovery of an endangered amphibian despite ongoing exposure to multiple stressors. *Proc. Natl. Acad. Sci. USA* **113**, 11889–11894 (2016).
14. LA Brannelly, et al., Mechanisms underlying host persistence following amphibian disease emergence determine appropriate management strategies. *Ecol. letters* **24**, 130–148 (2021).
15. RE Russell, GV DiRenzo, JA Szymanski, KE Alger, EH Grant, Principles and mechanisms of wildlife population persistence in the face of disease. *Front. Ecol. Evol.* **8**, 569016 (2020).
16. CL Searle, MR Christie, Evolutionary rescue in host-pathogen systems. *Evolution* **75**, 2948–2958 (2021).
17. AE Savage, KR Zamudio, Adaptive tolerance to a pathogenic fungus drives major histocompatibility complex evolution in natural amphibian populations. *Proc. Royal Soc. B: Biol. Sci.* **283**, 20153115 (2016).
18. B Epstein, et al., Rapid evolutionary response to a transmissible cancer in Tasmanian devils. *Nat. Commun.* **7**, 12684 (2016).
19. SA Gignoux-Wolfsohn, et al., Genomic signatures of selection in bats surviving white-nose syndrome. *Mol. Ecol.* **30**, 5643–5657 (2021).
20. OJ Holland, et al., Whole genome resequencing reveals signatures of rapid selection in a virus-affected commercial fishery. *Mol. Ecol.* **31**, 3658–3671 (2022).
21. R Medzhitov, DS Schneider, MP Soares, Disease tolerance as a defense strategy. *Science* **335**, 936–941 (2012).
22. JR Mendelson III, SM Whitfield, MJ Sredl, A recovery engine strategy for amphibian conservation in the context of disease. *Biol. Conserv.* **236**, 188–191 (2019).
23. MB Joseph, RA Knapp, Disease and climate effects on individuals drive post-reintroduction population dynamics of an endangered amphibian. *Ecosphere* **9**, e02499 (2018).
24. VT Vredenburg, et al., Concordant molecular and phenotypic data delineate new taxonomy and conservation priorities for the endangered mountain yellow-legged frog. *J. Zool.* **271**, 361–374 (2007).
25. J Grinnell, TI Storer, *Animal Life in the Yosemite.* (University of California Press), (1924).
26. DF Bradford, Allotopic distribution of native frogs and introduced fishes in high Sierra Nevada lakes of California: Implication of the negative effect of fish introductions. *Copeia* **1989**, 775–778 (1989).
27. RA Knapp, KR Matthews, Non-native fish introductions and the decline of the mountain yellow-legged frog from within protected areas. *Conserv. Biol.* **14**, 428–438 (2000).
28. VT Vredenburg, et al., Pathogen invasion history elucidates contemporary host pathogen dynamics. *PLOS ONE* **14**, e0219981 (2019).
29. VT Vredenburg, RA Knapp, TS Tunstall, CJ Briggs, Dynamics of an emerging disease drive large-scale amphibian population extinctions. *Proc. Natl. Acad. Sci. USA* **107**, 9689–9694 (2010).
30. LJ Rachowicz, et al., Emerging infectious disease as a proximate cause of amphibian mass mortality. *Ecology* **87**, 1671–1683 (2006).
31. RA Knapp, DM Boiano, VT Vredenburg, Removal of nonnative fish results in population expansion of a declining amphibian (mountain yellow-legged frog, *Rana muscosa*). *Biol. Conserv.* **135**, 11–20 (2007).
32. VT Vredenburg, Reversing introduced species effects: Experimental removal of introduced fish leads to rapid recovery of a declining frog. *Proc. Natl. Acad. Sci. USA* **101**, 7646–7650 (2004).
33. S Walker, et al., Environmental detection of *Batrachochytrium dendrobatidis* in a temperate climate. *Dis. Aquatic Org.* **77**, 105–112 (2007).
34. CJ Briggs, RA Knapp, VT Vredenburg, Enzootic and epizootic dynamics of the chytrid fungal pathogen of amphibians. *Proc. Natl. Acad. Sci. USA* **107**, 9695–9700 (2010).
35. H Zhou, T Hanson, R Knapp, Marginal Bayesian nonparametric model for time to disease arrival of threatened amphibian populations. *Biometrics* **71**, 1101–1110 (2015).
36. AP Rothstein, et al., Stepping into the past to conserve the future: Archived skin swabs from extant and extirpated populations inform genetic management of an endangered amphibian. *Mol. Ecol.* **29**, 2598–2611 (2020).
37. TJ Poorten, RA Knapp, EB Rosenblum, Population genetic structure of the endangered Sierra Nevada yellow-legged frog (*Rana sierrae*) in Yosemite National Park based on multi-locus nuclear data from swab samples. *Conserv. Genet.* **18**, 731–744 (2017).
38. Y Ohta, W Goetz, MZ Hossain, M Nonaka, MF Flajnik, Ancestral organization of the MHC revealed in the amphibian *Xenopus*. *The J. Immunol.* **176**, 3674–3685 (2006).
39. PJ Seddon, CJ Griffiths, PS Soorae, DP Armstrong, Reversing defaunation: Restoring species in a changing world. *Science* **345**, 406–412 (2014).
40. RA Knapp, CJ Briggs, TC Smith, JR Maurer, Nowhere to hide: impact of a temperature-sensitive amphibian pathogen along an elevation gradient in the temperate zone. *Ecosphere* **2**, art93 (2011).
41. KR Zamudio, CA McDonald, AM Belasen, High variability in infection mechanisms and host responses: a review of functional genomic studies of amphibian chytridiomycosis. *Herpetologica* **76**, 189 (2020).
42. AE Savage, KR Zamudio, MHC genotypes associate with resistance to a frog-killing fungus. *Proc. Natl. Acad. Sci. USA* **108**, 16705–16710 (2011).
43. A Bataille, et al., Susceptibility of amphibians to chytridiomycosis is associated with MHC class II conformation. *Proc. Royal Soc. B: Biol. Sci.* **282**, 20143127 (2015).
44. LF Grogan, et al., Evolution of resistance to chytridiomycosis is associated with a robust early immune response. *Mol. Ecol.* **27**, 919–934 (2018).
45. AR Ellison, et al., More than skin deep: functional genomic basis for resistance to amphibian chytridiomycosis. *Genome Biol. Evol.* **7**, 286–298 (2014).
46. D Robledo, A Hamilton, AP Gutiérrez, JE Bron, RD Houston, Characterising the mechanisms underlying genetic resistance to amoebic gill disease in Atlantic salmon using RNA sequencing. *BMC Genomics* **21** (2020).
47. D Robledo, O Matika, A Hamilton, RD Houston, Genome-wide association and genomic selection for resistance to amoebic gill disease in Atlantic salmon. *G3 Genes|Genomes|Genetics* **8**, 1195–1203 (2018).
48. M Soejima, et al., Nucleotide sequence analyses of human complement 6 (C6) gene suggest balancing selection. *Annals Hum. Genet.* **69**, 239–252 (2005).
49. T Fukazawa, Y Naora, T Kunieda, T Kubo, Suppression of the immune response potentiates tadpole tail regeneration during the refractory period. *Development* **136**, 2323–2327 (2009).
50. C Dodd Jr, Amphibian conservation and population manipulation in *Status and conservation of US amphibians*, ed. M Lannoo. (Universiy of California Press), pp. 265–270 (2005).
51. S Ellison, RA Knapp, W Sparagon, A Swei, VT Vredenburg, Reduced skin bacterial diversity correlates with increased pathogen infection intensity in an endangered amphibian host. *Mol. Ecol.* **28**, 127–140 (2018).
52. JE Humphries, et al., Do immune system changes at metamorphosis predict vulnerability to chytridiomycosis? an update. *Developmental and Comparative Immunology* **136**, 104510 (2022).
53. M Hollanders, LF Grogan, CJ Nock, HI McCallum, DA Newell, Recovered frog populations coexist with endemic *batrachochytrium dendrobatidis* despite load-dependent mortality. *Ecol. Appl.* **33** (2022).
54. TWJ Garner, et al., Mitigating amphibian chytridiomycoses in nature. *Philos. Transactions Royal Soc. B: Biol. Sci.* **371**, 20160207 (2016).
55. RA Knapp, et al., Effectiveness of antifungal treatments during chytridiomycosis epizootics in populations of an endangered frog. *PeerJ* **10**, e12712 (2022).
56. BC Scheele, et al., After the epidemic: Ongoing declines, stabilizations and recoveries in amphibians afflicted by chytridiomycosis. *Biol. Conserv.* **206**, 37–46 (2017).
57. LS Mills, et al., Winter color polymorphisms identify global hot spots for evolutionary rescue from climate change. *Science* **359**, 1033–1036 (2018).
58. EM Oziolor, et al., Adaptive introgression enables evolutionary rescue from extreme environmental pollution. *Science* **364**, 455–457 (2019).
59. T Broquet, L Berset-Braendli, G Emaresi, L Fumagalli, Buccal swabs allow efficient and reliable microsatellite genotyping in amphibians. *Conserv. Genet.* **8**, 509–511 (2007).
60. S Chen, Y Zhou, Y Chen, J Gu, fastp: an ultra-fast all-in-one fastq preprocessor. *Bioinformatics* **34**, i884–i890 (2018).
61. T Hon, et al., Highly accurate long-read hifi sequencing data for five complex genomes. *Sci. Data* **7** (2020).
62. H Li, Aligning sequence reads, clone sequences and assembly contigs with bwa-mem (2013).
63. GA Van der Auwera, BD O'Connor, *Genomics in the cloud: using Docker, GATK, and WDL in Terra.* (O'Reilly Media), p. 496 (2020).
64. T Jombart, *adegenet*: a R package for the multivariate analysis of genetic markers. *Bioinformatics* **24**, 1403–1405 (2008).
65. AR Quinlan, IM Hall, BEDTools: a flexible suite of utilities for comparing genomic features. *Bioinformatics* **26**, 841–842 (2010).
66. S Altschul, Gapped blast and psi-blast: a new generation of protein database search programs. *Nucleic Acids Res.* **25**, 3389–3402 (1997).
67. M Kearse, et al., Geneious Basic: An integrated and extendable desktop software platform for the organization and analysis of sequence data. *Bioinformatics* **28**, 1647–1649 (2012).
68. P Danecek, et al., The variant call format and VCFtools. *Bioinformatics* **27**, 2156–2158 (2011).
69. AP Bishop, EA Chambers, IJ Wang, Generating continuous maps of genetic diversity using moving windows. *Methods Ecol. Evol.* (2023).
70. TM Beissinger, GJ Rosa, SM Kaeppler, D Gianola, N de Leon, Defining window-boundaries for genomic analyses using smoothing spline techniques. *Genet. Sel. Evol.* **47**, 1–9 (2015).
71. A Conesa, et al., Blast2GO: a universal tool for annotation, visualization and analysis in functional genomics research. *Bioinformatics* **21**, 3674–3676 (2005).
72. RA Knapp, Effects of nonnative fish and habitat characteristics on lentic herpetofauna in Yosemite National Park, usa. *Biol. Conserv.* **121**, 265–279 (2005).
73. MB Joseph, mrmr: mark recapture miscellany in R (2019) R package version 0.1.1.
74. R Core Team, *R: A Language and Environment for Statistical Computing* (R Foundation for Statistical Computing, Vienna, Austria), (2022).
75. B Goodrich, J Gabry, I Ali, S Brilleman, rstanarm: Bayesian applied regression modeling via Stan. (2022) R package version 2.21.3.
76. A Gelman, et al., *Bayesian Data Analysis.* (CRC Press), (2013).
77. J Gabry, D Simpson, A Vehtari, M Betancourt, A Gelman, Visualization in Bayesian workflow. *J. Royal Stat. Soc. Ser. A* **182**, 389–402 (2019).
78. A Vehtari, A Gelman, J Gabry, Practical Bayesian model evaluation using leave-one-out cross-validation and WAIC. *Stat. Comput.* **27**, 1413–1432 (2016).
79. A Vehtari, et al., loo: Efficient leave-one-out cross-validation and waic for Bayesian models (2022) R package version 2.5.1.
80. D Boyle, D Boyle, V Olsen, J Morgan, A Hyatt, Rapid quantitative detection of chytridiomycosis (*Batrachochytrium dendrobatidis*) in amphibian samples using real-time Taqman PCR assay. *Dis. Aquatic Org.* **60**, 141–148 (2004).
81. MQ Wilber, RA Knapp, TC Smith, CJ Briggs, Host density has limited effects on pathogen invasion, disease-induced declines and within-host infection dynamics across a landscape of disease. *J. Animal Ecol.* **91**, 2451–2464 (2022).

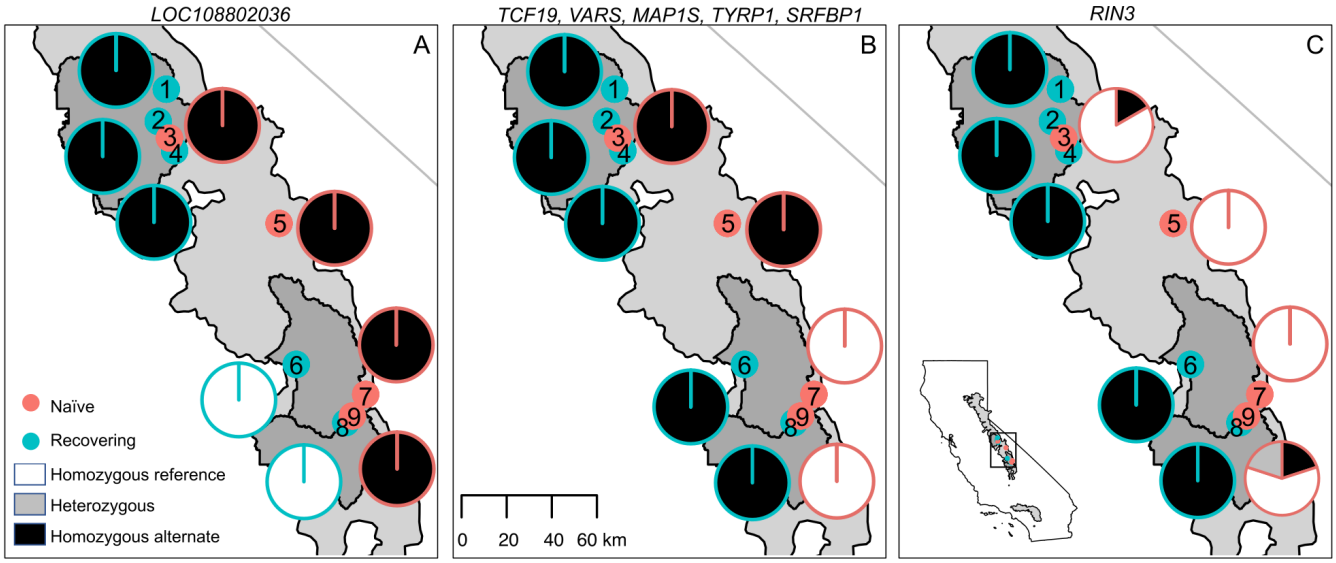

Fig. 1. Evidence for selection in recovering MYL frog populations at the landscape scale. For each of the 9 naive and recovering MYL frog populations, pie charts show allele frequencies for the 11 outlier SNPs from 7 distinct genes: (A) LOC108802036, (B) TCF19, VARS, MAP1S, TYRP1, SRFBP1, and (C) RIN3. Charts are superimposed on a map of the Sierra Nevada study area, with Yosemite, Kings Canyon, and Sequoia National Parks (from north to south) shown in dark gray, and the range boundary for MYL frogs in this portion of the Sierra Nevada shown in light gray. The inset map locates the study area in California.

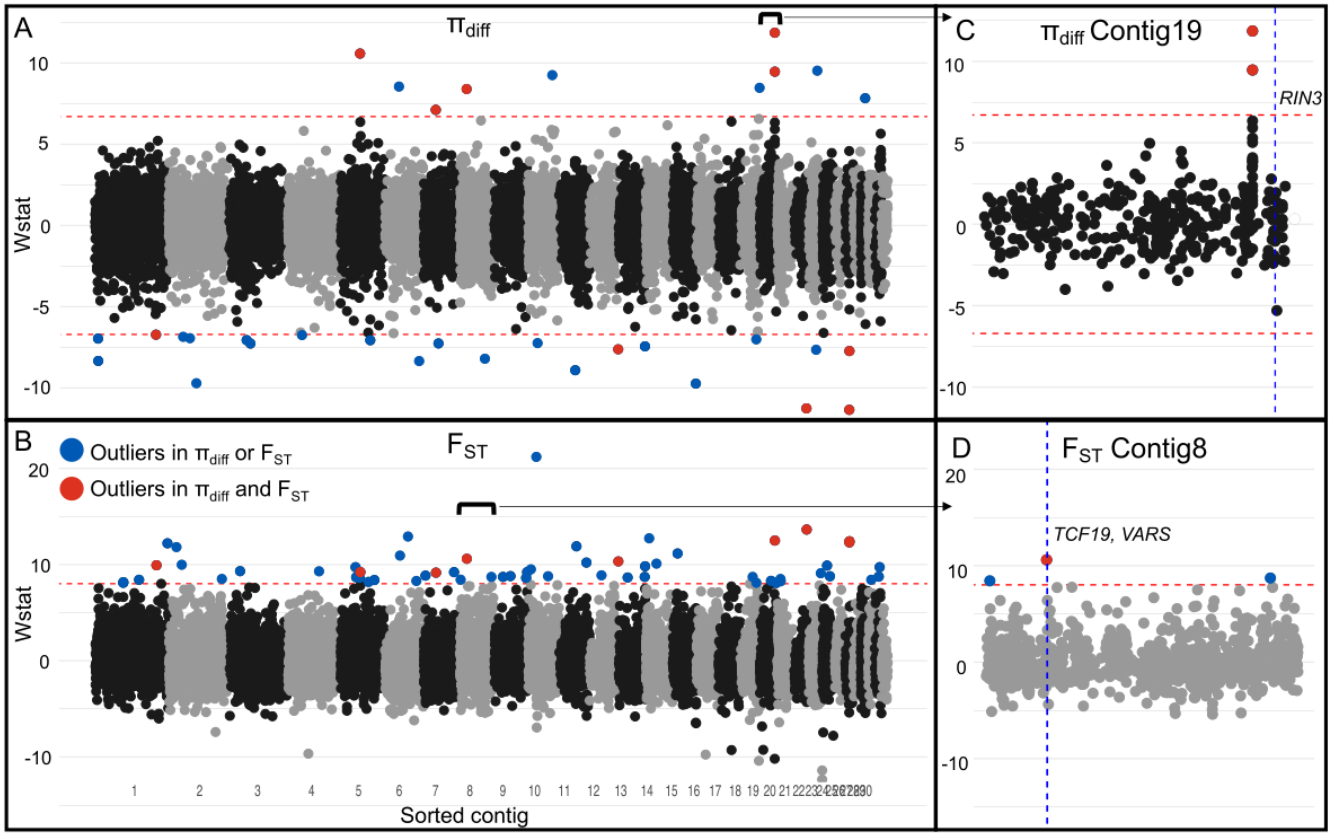

Fig. 2. Evidence for selection on genomic regions in recovering MYL frog populations. Results are from the splined window analysis and show outlier windows for the difference in (A) nucleotide diversity π_{diff} and (B) F_{ST}. Outlier regions for either π_{diff} or F_{ST} are shown in blue and outlier regions for both π_{diff} and F_{ST} are shown in red. (C) Magnified Contig19 from (A) showing two adjacent outlier windows for π_{diff} 12.9Mb upstream of the RIN3 outlier SNP (indicated with a dashed vertical blue line). (D) Magnified Contig8 from from (B) showing the F_{ST} outlier window that includes the outlier SNPs TCF19 and VARS. This region of the genome contains 8 annotated genes known to occur in the extended MHC Class I and III regions.

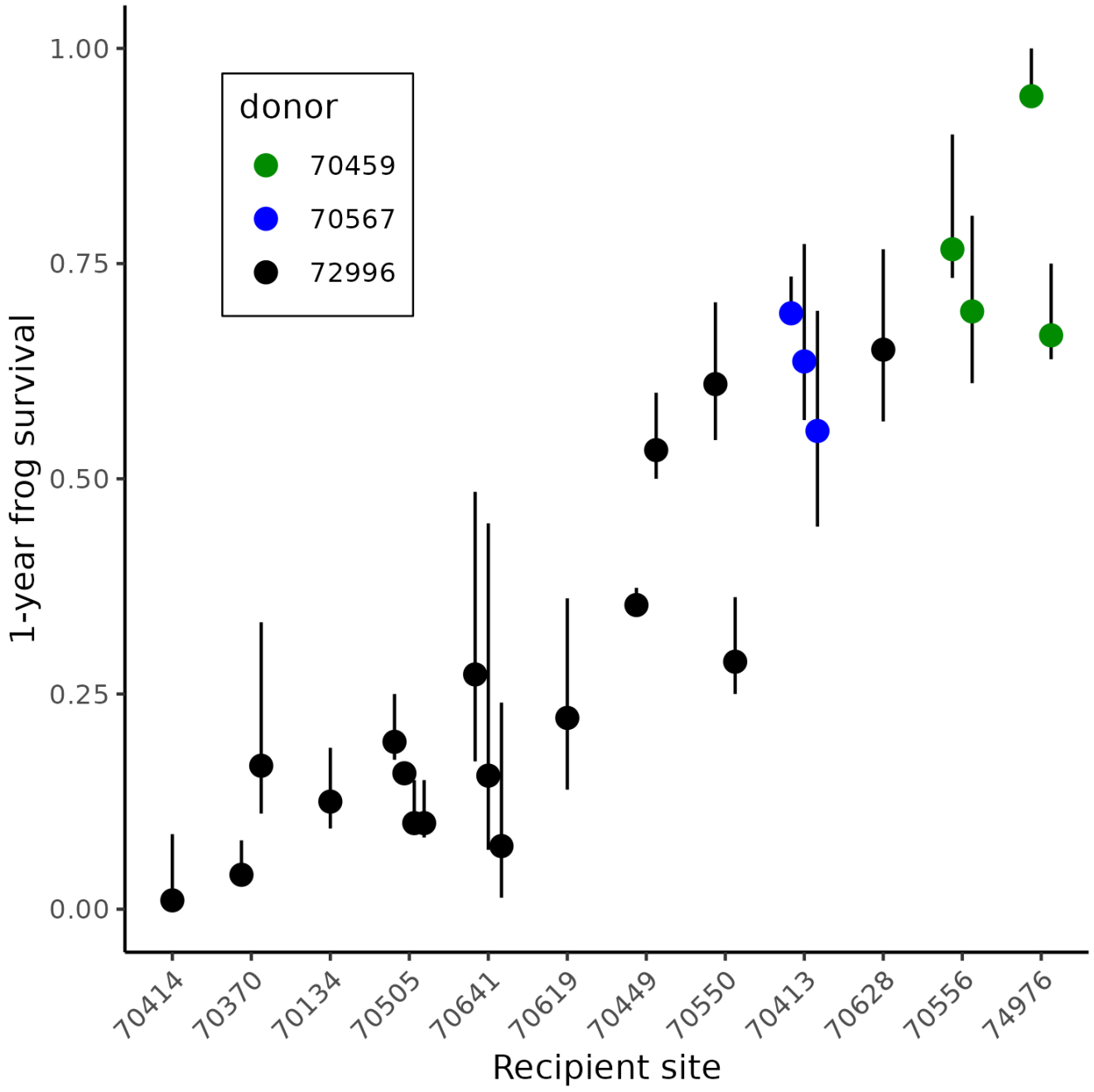

Fig. 3. Evidence for frog survival at the recipient sites following translocation. Median 1-year survival for each cohort of translocated frogs at the 12 recipient sites. Sites are arranged along the x-axis using the average of the median 1-year survival per translocation at each site. Dot colors indicate the donor population from which frogs in each translocated cohort were collected. Error bars show the 95% uncertainty intervals. When multiple translocations were conducted to a site, points and error bars are slightly offset to avoid overlap.

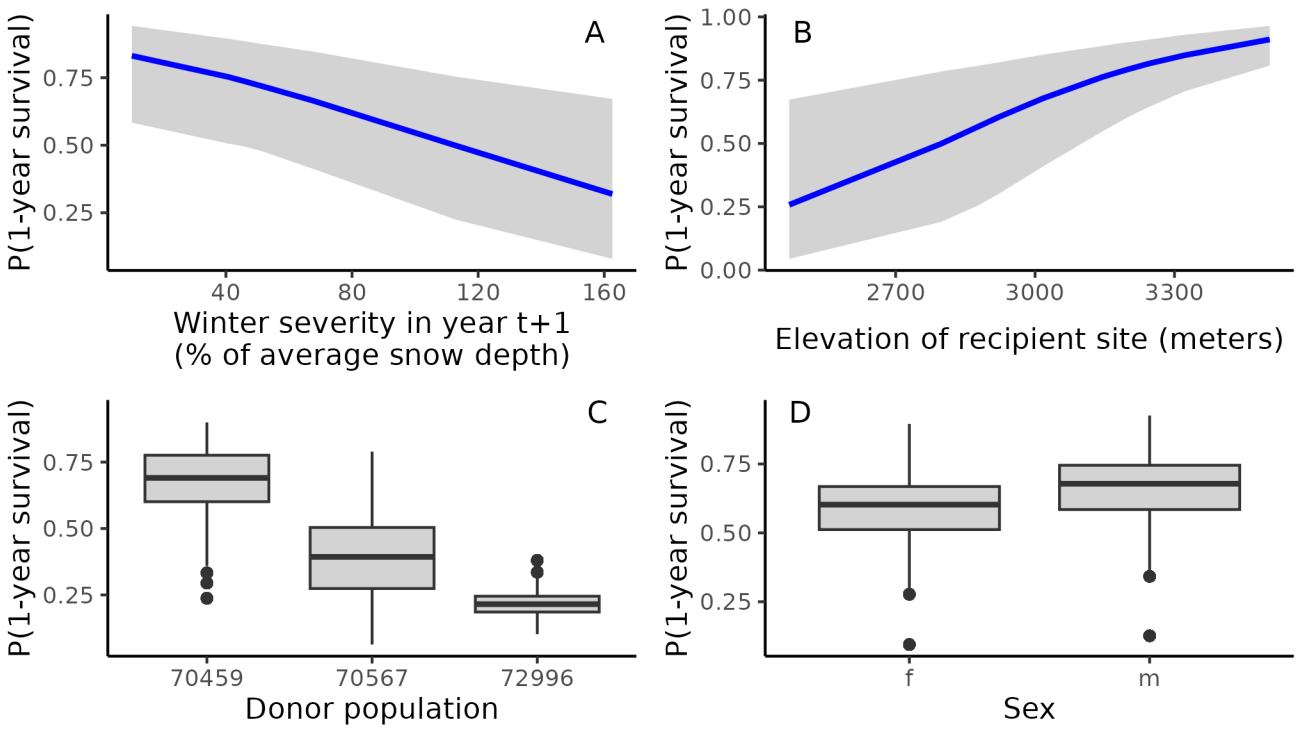

Fig. 4. Evidence for reduced impacts of Bd on MYL frogs as indicated by the lack of an effect of Bd load on survival. Results show conditional effects of the important predictors of 1-year frog survival (survival is expressed as a probability). (A) winter severity in the year following translocation, (B) elevation of recipient site, (C) donor population, and (D) sex. In (A) and (B), blue lines are medians and gray ribbons are 95% uncertainty intervals. In (C) and (D), box plots show medians, first and third quartiles, largest and smallest values within 1.5x interquartile range, and values outside the 1.5x interquartile range.

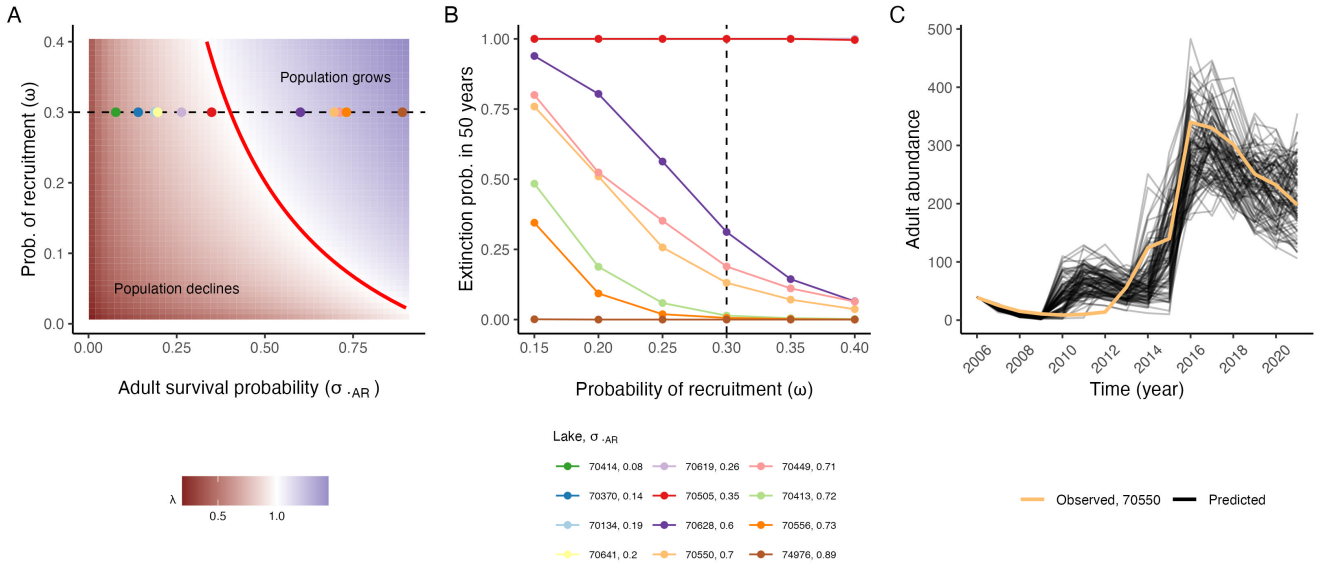

Fig. 5. Predicted and observed growth and persistence of translocated populations. Population viability analysis of translocated MYL frogs quantified the long-run growth rate and extinction probability of frog populations: (A) Predicted long-run growth rate λ for different values of yearly adult survival probability σ_{A_R} and probability of recruitment ω, given the parameterized, deterministic model. Colored points show the predicted λ values for the twelve translocated populations when probability of recruitment into the adult class is $\omega = 0.3$ (indicated by the dashed line). The red line shows where $\lambda = 1$. (B) Predicted 50-year extinction probabilities of the 12 translocated populations given demographic stochasticity, environmental variability in ω, and different mean values of ω. The dashed line shows where $\omega = 0.3$, for comparison to (A). There are 6 lines at extinction probability = 1, 5 of which (70414–70619) are hidden beneath the line for 70505. (C) 100 simulated trajectories (black lines) from the population viability model that most closely matched the observed abundance trajectory of adult amphibians at site 70550 (light orange).